Archival Report

Biological Psychiatry

Large-scale Persistent Network Reconfiguration Induced by Ketamine in Anesthetized Monkeys: Relevance to Mood Disorders

Qian Lv, Liqin Yang, Guoliang Li, Zhiwei Wang, Zhuangming Shen, Wenwen Yu, Qinying Jiang, Baoyu Hou, Jian Pu, Hailan Hu, and Zheng Wang

ABSTRACT

BACKGROUND: Ketamine is a highly attractive candidate for developing fast-onset antidepressant agents; however, the relevant brain circuits that underlie sustained, efficacious antidepressant effects remain largely unknown.

METHODS: We used a holistic scheme combining whole-brain resting-state fMRI and graph theoretical analysis to examine the sustained effects on brain networks after administration of a single dose of ketamine and to identify the brain regions and circuits preferentially targeted by ketamine. Topological differences in functional networks of anesthetized macaque monkeys were compared between ketamine (.5 mg/kg) and saline treatment after 18 hours.

RESULTS: We observed persistent global reconfiguration of small-world properties in response to ketamine intake, accompanied by large-scale downregulation of functional connectivity, most prominently in the orbital prefrontal cortex, the subgenual and posterior cingulate cortices, and the nucleus accumbens. Intriguingly, intrinsic connectivity with the medial prefrontal areas in the reward circuits were selectively downregulated. Global and regional regulations of the brain networks precisely opposed the maladaptive alterations in the depressed brain.

CONCLUSIONS: Our results demonstrated that local synaptic plasticity triggered by blockade of *N*-methyl-D-aspartic acid receptors was capable of translating into prolonged network reconfiguration in the distributed cortico-limbic-striatal circuit, providing mechanistic insight into developing specific loci or circuit-targeted, long-term therapeutics.

Keywords: Functional connectivity, Graph theory, Ketamine, Macaque monkey, Mood disorders, Neural network plasticity

http://dx.doi.org/10.1016/j.biopsych.2015.02.028

Mood disorders, such as major depressive disorder (MDD), are likely accompanied by distributed system-level disturbances in brain circuitry (1–6). There is increasing recognition that therapeutic interventions could generate structural and functional network reorganization through the possible neural plasticity (4,7) and regulate system-level abnormalities in the brain, eventually leading to complete rehabilitation. Converging evidence has demonstrated that a single subanesthetic dose of ketamine, a noncompetitive *N*-methyl-D-aspartic acid (NMDA) receptor antagonist, produces a rapid-acting and long-lasting antidepressant response (8–13) attributable to synaptic plasticity rather than simple antagonism of NMDA receptors (7,11). These features are extremely attractive for novel pharmacological strategies (14) and have inspired a flurry of preclinical and clinical studies of the neurobiological mechanisms of ketamine action (15,16). To date, however, several key questions regarding the antidepressant action of ketamine remain largely unsolved. First, what are the relevant brain circuits that underlie the long-term, efficacious action of ketamine? Second, why do many patients show a response 24 hours after ketamine administration? (17). Accordingly, is there sustained neural network reconfiguration after acute ketamine treatment, considering the metabolic half-life of ketamine is shorter than 3 to 4 hours? (18). Finally, although synaptic plasticity triggered by the transient blockade of NMDA receptors could help restore disrupted homeostatic regulation and lost synaptic connections (4,7,11), the involved brain regions where synaptic plasticity occurs in complex mood and emotion circuitry, thereby contributing to long-lasting antidepressant effects, remains unknown.

To address these questions, we tested the therapeutic effects of a single dose of ketamine on healthy adult macaque monkeys. Growing evidence has validated the use of resting-state functional magnetic resonance imaging (rsfMRI) in anesthetized macaques (19–27) and has underscored its potential to bridge information between human and animal models (28–31). Although the effect of anesthetic agents on functional brain networks remains poorly understood, recent study has demonstrated that stable functional connectivity patterns under a narrow range of medium level isoflurane

ISSN: 0006-3223

(e.g., ±.25%) are suitable for anesthetized nonhuman primate investigations (26). Furthermore, whole-brain rsfMRI allows unbiased, simultaneous identification of all pharmacologically affected regions in the brain. Through transiently and reversibly controlled neurochemical perturbations, nonhuman primate models may serve as ideal testing benchmarks to clarify the underlying biomechanisms of drug action in the absence of any pre-existing homeostatic dysfunction as part of the complex disease process (e.g., multidimensional symptomatology in psychiatric disorders), comorbidity, or medication status.

Given the ubiquitous distribution of NMDA receptors throughout the brain (14), a randomized, placebo-controlled functional connectome study was conducted in anesthetized monkeys 18 hours after ketamine and saline administration. The dose used (.5 mg per kg) has achieved clinically meaningful improvements in MDD patients (8–10,17), and the time point was chosen for the most prominent antidepressant response (9), without additional schizophrenia-like symptoms (32). Although recent rsfMRI studies have evaluated the antidepressant effects of ketamine at a priori selection of candidate brain regions or pathways (33–35), a global view of the action of ketamine on the whole-brain scale is still lacking. Therefore, we applied graph theoretical analysis to quantitatively examine the overall topological organization of brain networks (36) and used network-based statistics (NBS) (37) to characterize specific features within a network. This study represents the first fMRI investigation of the antidepressant effects of ketamine in nonhuman primates, using a holistic scheme that could possibly identify hitherto unidentified systems relevant to novel therapeutic targets in the brain reward circuitry. Our primary hypotheses were that a single subanesthetic dose of ketamine would produce sustained network reconfiguration in healthy subjects after it was metabolically eliminated and that this prolonged action, which counteracts abnormalities of functional networks in MDD patients, would provide a plausible mechanistic underpinning for the long-term antidepressant effects of ketamine.

METHODS AND MATERIALS

Animal Preparation

All experimental procedures in nonhuman primate research in this study were approved by the Institute of Neuroscience Animal Care and Use Committee and by the Shanghai Institute for Biological Sciences Biomedical Research Ethics Committee and conformed to the National Institutes of Health guidelines for the humane care and use of laboratory animals.

Nine adult macaque monkeys (3 male and 1 female *Macaca fascicularis* and 5 male *Macaca mulatta*) weighing 5.0 to 10.0 kg (7.7 ± 1.8 kg) were prepared and maintained for fMRI scans. Animals were intramuscularly injected with either a single subanesthetic dose of ketamine (.5 mg per kg) or placebo saline (.90% w/v of NaCl) in random order (Figure 1A). In light of previous nonhuman primate (38) and human clinical studies (17), the ketamine dose was determined to produce sufficient regulatory effects in subjects. Follow-up fMRI scans were scheduled 18 hours after ketamine or saline administration. The imaging interval between saline and ketamine administration was spaced at least 1 month apart to avoid possible carry-over effects. Before each scanning session, an anesthesia cocktail of dexmedetomidine (18–30 μg per kg) and midazolam (.2–.3 mg per kg), supplemented with atropine sulfate (.05 mg per kg), was introduced to the animals. After monkeys were intubated, under an anesthesiologist's guidance (GL), the anesthesia was maintained using the lowest possible concentration of isoflurane gas. For all animal scans, the mean (±SD) inhaled concentration was .92% (±.26%). Subjects received intermittent positive pressure ventilation by an MRI-compatible ventilator (CWE Inc., Weston, Wisconsin) to ensure a constant respiration rate (31.8 ± 2.3 breaths/min). Vital signs, including blood oxygenation, rectal temperature, heart rate (Small Animal Instruments Inc., Stonybrook, New York), respiration rate, and end-tidal CO_2 (Smiths Medical ASD Inc., Dublin, Ohio), were continuously monitored during the experiment and maintained tightly within normal limits. Oxygen saturation was maintained over 95%, and body temperature was kept constant using a hot water blanket (Gaymar Industries Inc., Orchard Park, New York). Lactated Ringer's solution was given at 10 mL per kg per hour during the anesthesia procedure.

Image Acquisition

A cohort of image data was acquired from the Institute of Neuroscience on a 3-T whole-body scanner (Siemens Healthcare, Germany) running with or without an enhanced gradient coil insert (AC88; 80 mT/m maximum gradient strength, 800 $mT \cdot m^{-1} \cdot s^{-1}$ maximum slew rate). A total of 57 of 96 imaging datasets were obtained from the standard Trio system, using a protocol similar to that used with AC88. Two sets of custom-made 8-channel phased-array transceiver coils were used for the imaging sessions on the AC88 and Trio systems (provided by Dr. Lawrence Wald's laboratory at Massachusetts General Hospital, Boston, Massachusetts, and developed in-house), respectively.

Whole-brain resting-state fMRI data were collected using a gradient-echo echo-planar imaging (EPI) sequence (TR = 2000 ms; TE = 29 ms; flip angle = 77°; slices = 32; field of view = 96 × 96 mm; 1.5 × 1.5 mm^2 in plane resolution; slice thickness = 2.5 mm; GRAPPA factor = 2). For each experiment, 4 to 6 EPI runs were acquired, and each run contained 200 functional volumes. A pair of gradient echo images (echo time: 4.22 ms and 6.68 ms, respectively) with the same orientation and resolution as the EPI images were acquired to generate a field map for distortion correction of the EPI images. High-resolution T1-weighted anatomical images were acquired using an MPRAGE sequence (TR = 2500 ms; TE = 3.12 ms; TI = 1100 ms; flip angle = 9°; acquisition voxel size = .5 × .5 × .5 mm^3; 144 sagittal slices). Six whole-brain anatomical runs were acquired and averaged for better brain segmentation and three-dimensional cortical reconstruction. Each experiment lasted for approximately 3 to 4 hours, and a total of 96 imaging datasets (47 for ketamine condition and 49 for saline condition) were collected from 9 monkeys.

Network Construction

Node and Edge Definition. A network is composed of nodes and edges between nodes. Herein, nodes represent

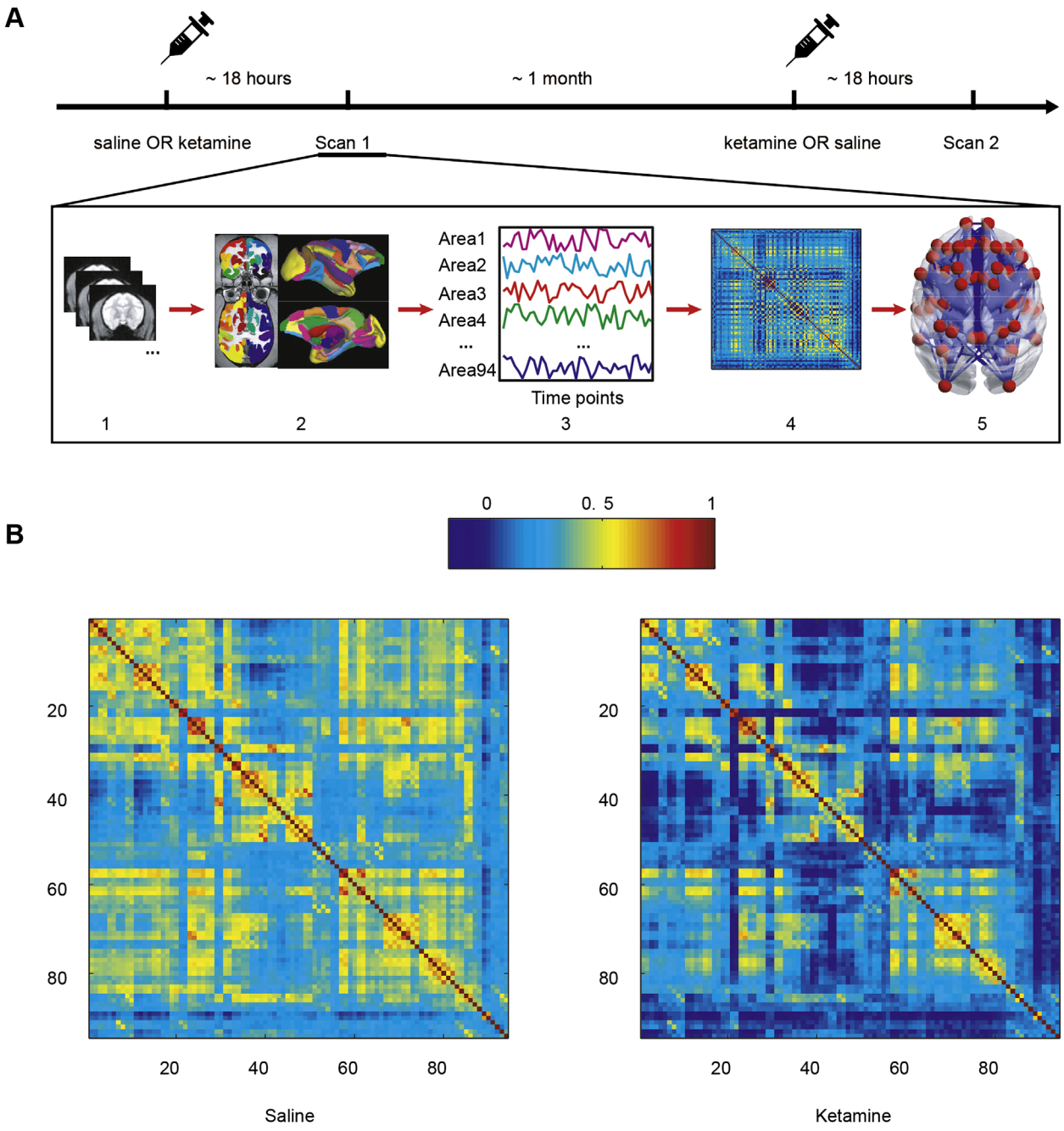

Figure 1. Resting state functional brain connectome study of ketamine. (**A**, upper panel) The experimental paradigm. Each animal functional magnetic resonance imaging (fMRI) scan was scheduled 18 hours after a single dose administration of ketamine or saline was given in random order. The scan interval between the saline and ketamine treatments was spaced at least 1 month apart to avoid any carry-over effects. (**A**, lower panel) Flow chart of graph theoretical analysis. Panel 1: resting-state fMRI data were acquired from anesthetized monkeys. Panel 2; Entire monkey brain was charted with 94 regions, including 78 cortical and 16 subcortical regions. Panels 3 and 4: Mean time courses of each brain region were calculated and subjected to region-specific Pearson correlation, resulting in a 94 × 94 correlation matrix. Panel 5: Topological features of the correlation matrices after ketamine and saline administration were analyzed and statistically compared. (**B**) Grand mean correlation matrices of saline and ketamine regimen groups.

brain regions, and edges represent the statistical correlation in fMRI signals across different regions. To define the monkey brain nodes, the regional map cortical parcellation was mapped onto the F99 macaque standard surface template (39) and transformed to voxel space with a 2-mm extrusion using Caret software (http://www.nitrc.org/projects/caret/). To construct a complete brain network, we further collated the subcortical parcellation of the macaque monkey from the INIA19 template (40), which included the caudate, putamen, thalamus, hypothalamus, nucleus accumbens (NAc) and globus pallidus

(amygdala and hippocampus were included in the regional map cortical parcellation [see Supplementary Table S1 for the complete anatomical labels of all brain regions]). Thus, our anatomical template contained a total of 94 brain regions, 47 of which were mirrored from one hemisphere to the other. To define the network edges, we calculated region-wise Pearson correlation coefficients and generated a 94 × 94 correlation matrix for each imaging dataset (Figure 1B shows the grand mean correlation matrices of ketamine and saline groups). The mean time series of each region (node) was obtained by averaging the time series of all voxels within that region.

Threshold Selection. As there is no current consensus on the selection of network thresholds in graph theoretical analysis, network sparsity was determined as the threshold according to previous studies (41,42). Sparsity level *S,* defined as the ratio of the number of existing edges divided by the maximum possible number of edges in a network, was applied to all correlation matrices. This treatment normalized all resultant networks to have the same number of edges and minimized the effects of possible discrepancies in the overall correlation strength between groups. Practically, the threshold for each correlation matrix was determined repeatedly over a wide range of sparsity levels with an increment of .01 according to two criteria: 1) that the average degree (node degree is the number of connections linked to the node) over all nodes of each threshold network was larger than $2 \times \log(N)$ (where $N = 94$ here); and 2) that the normalized clustering coefficient γ, and the normalized characteristic path length λ, fulfilled the criteria of $[\gamma > 1]$ and $[\lambda \approx 1]$ for all individuals (43). This data-driven procedure guaranteed that the threshold networks were biologically plausible, showing the properties of small-worldness, and held sparse properties with as few spurious edges as possible (41). After preprocessing and network construction (see Supplementary Material for details), 76 imaging datasets entered the subsequent statistical comparisons.

Global and Regional Properties Analysis

The Brain Connectivity Toolbox (44) and GRETNA software were used to investigate the topological features of the functional networks constructed at each sparsity level within the data-derived sparsity range S (.1 ∼ .3). The global measures included 1) small-world parameters involving the clustering coefficient C_p, characteristic path length L_p, γ, λ, and small-worldness σ; and 2) network efficiency involving local efficiency E_{loc}, and global efficiency E_{glob} (see Supplement 1 for details). For the calculation of γ and λ, 100 random networks were generated for each weighted network, using a modified Maslov's wiring program, which preserved the original weight of each node during normalization (45). Nonparametric permutation tests (10,000 permutations) for global differences in these topological metrics at each sparsity level (.1 ∼ .3, step increment = .01) were tested for significance with an false discovery rate (FDR) of 5%. To avoid multiple comparison problems, the area under the curve for each network metric within the chosen sparsity range was also computed for statistical comparison (41,46). For regional measurements, we calculated the connectivity strength of each node and compared differences between the two conditions (permutation tests with FDR of 5%).

Functional Connectivity Analysis

To further localize specific pairs of brain regions in which functional connectivity was altered after ketamine application, the NBS approach was used to seek between-group differences (37). The NBS approach copes with the multiple comparison problems of comparing connection data with $[N \times (N - 1)/2]$ connections. The correction strategy is analogous to cluster-based strategies used in voxel-wise MRI data analysis by evaluating the null hypothesis at the level of connected subnetworks rather than individual connections. In this method, subnetworks were identified with a strategy similar to identifying significant clusters in fMRI analysis (see Supplement 1 for details), and connections in subnetworks that were significant at a corrected level of $p < .05$ were reported.

RESULTS

Ketamine-related Regulations of Small-World Properties

We determined a data-specific small-world regimen at a sparsity range of $.1 \leq S \leq .3$ to construct a simplified graphic network model consisting of brain regions (nodes) and connections (edges drawn between nodes to represent functional connectivity) (Figure 1B). We began by examining the small-world properties of the networks (Figure 1B) and observed that functional networks of both saline and ketamine conditions possessed typical features of small-worldness (i.e., $\gamma > 1$ and $\lambda \approx 1$) (Figure S2 in Supplement 1). In comparison to saline treatment, the ketamine group consistently showed significant decreases in C_p (FDR-corrected $p < .05$), E_{loc} (FDR-corrected $p < .05$), and E_{glob} (FDR-corrected $p < .005$) (Figure 2A,2F, 2G), and significant increases in L_p (FDR-corrected $p < .0005$) and λ (FDR-corrected $p < .05$) at each sparsity level (Figure 2B,2D). Neither changes in γ (FDR-corrected $p = .14$) nor in σ (FDR-corrected $p = .35$) between the two groups were statistically significant (Figure 2C,2E). These findings were confirmed by comparing the parameter area under the curve of each global network metric (Figure 2H).

Ketamine-related Regulations of Regional Nodal Strength

The connectivity strength of each node was compared between the two conditions, showing that ketamine produced substantial downregulation (Figure 3, cold colors) and upregulation (Figure 3, warm colors) in widely distributed brain regions (Figure 3 and Table S2). For simplicity, we categorized the affected brain nodes into two main classes by their significance levels. The most striking reduction in connectivity strength occurred in the bilateral orbital (orbitoinferior and orbitomedial) frontal cortices (OFC), striatum (bilateral caudate and putamen), bilateral globus pallidum, right gustatory cortex, right secondary somatosensory cortex and limbic structures including the left anterior cingulate cortex (ACC), right posterior insula, and bilateral hippocampus, parahippocampus, and

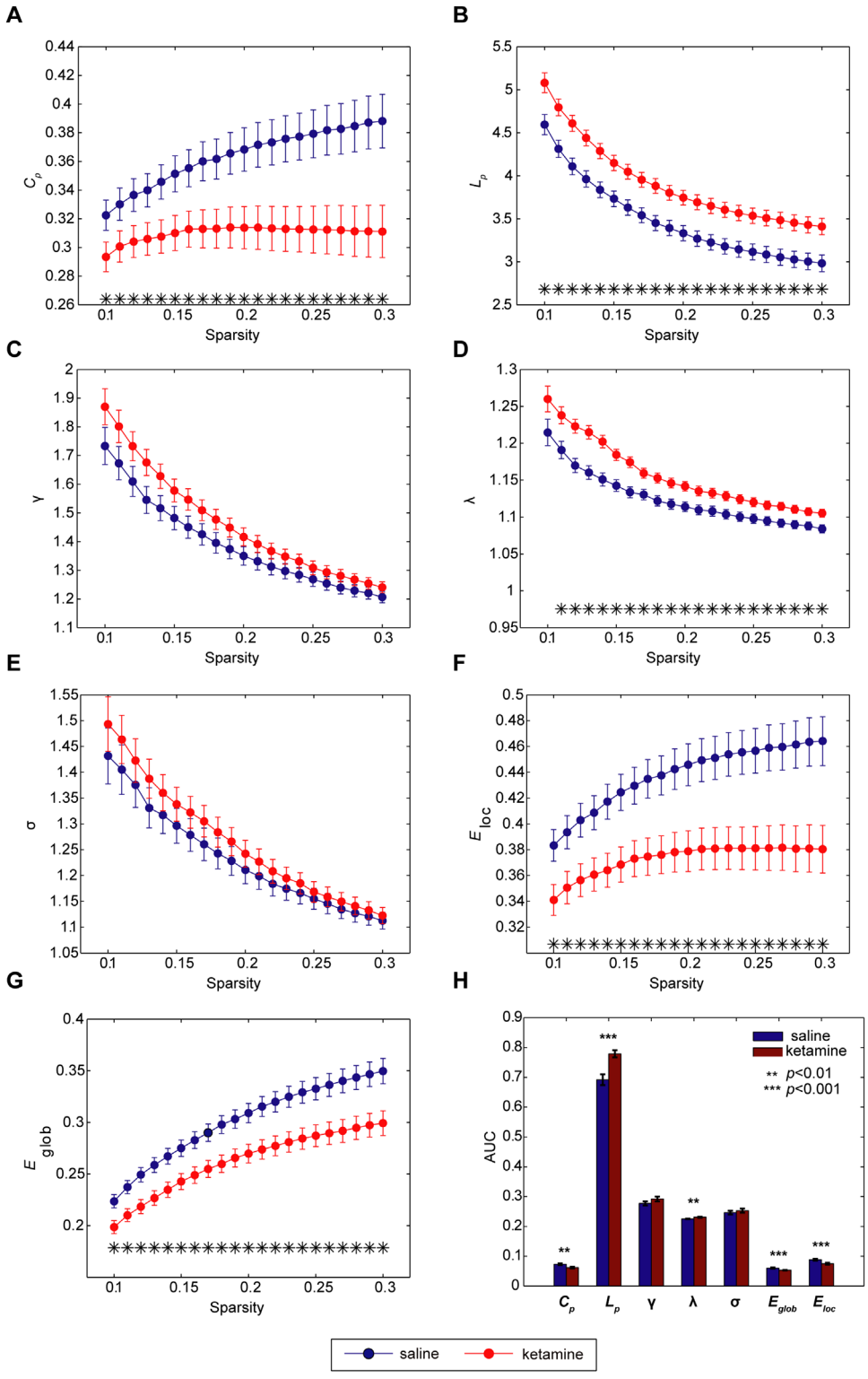

Figure 2. Ketamine-related regulations of global small-world properties of functional brain network. **(A–G)** Small-world properties were plotted as a function of sparsity level, S, within the small-world regimen of $.10 \leq S \leq .30$. Asterisks in the plot denote significant group differences (false discovery rate corrected, $p < .05$). **(H)** Altered area under the curve (AUC) of small-world network properties in the ketamine group compared to the saline group. Significant differences were found between the clustering coefficient C_p ($p = .0035$), the shortest path length L_p ($p = .0001$), the normalized shortest path length λ ($p = .0061$), the global efficiency E_{glob} ($p = .0001$), and the local efficiency E_{loc} ($p = .0006$) values of the saline group and those of the ketamine group. Error bars are standard errors of the mean.

thalamus (FDR-corrected $p < .01$). Modest but significant decreases were found in the right ACC, left posterior cingulate cortex (PCC), sensory areas (somatosensory, visual, auditory, motor and gustatory cortices), right ventrolateral premotor, left medial prefrontal cortex (PFC), and right ventral temporal cortex (FDR-corrected $p < .05$). In contrast, brain nodes with increased connectivity strength were restricted to the left superior and inferior parietal cortices (FDR-corrected $p < .05$).

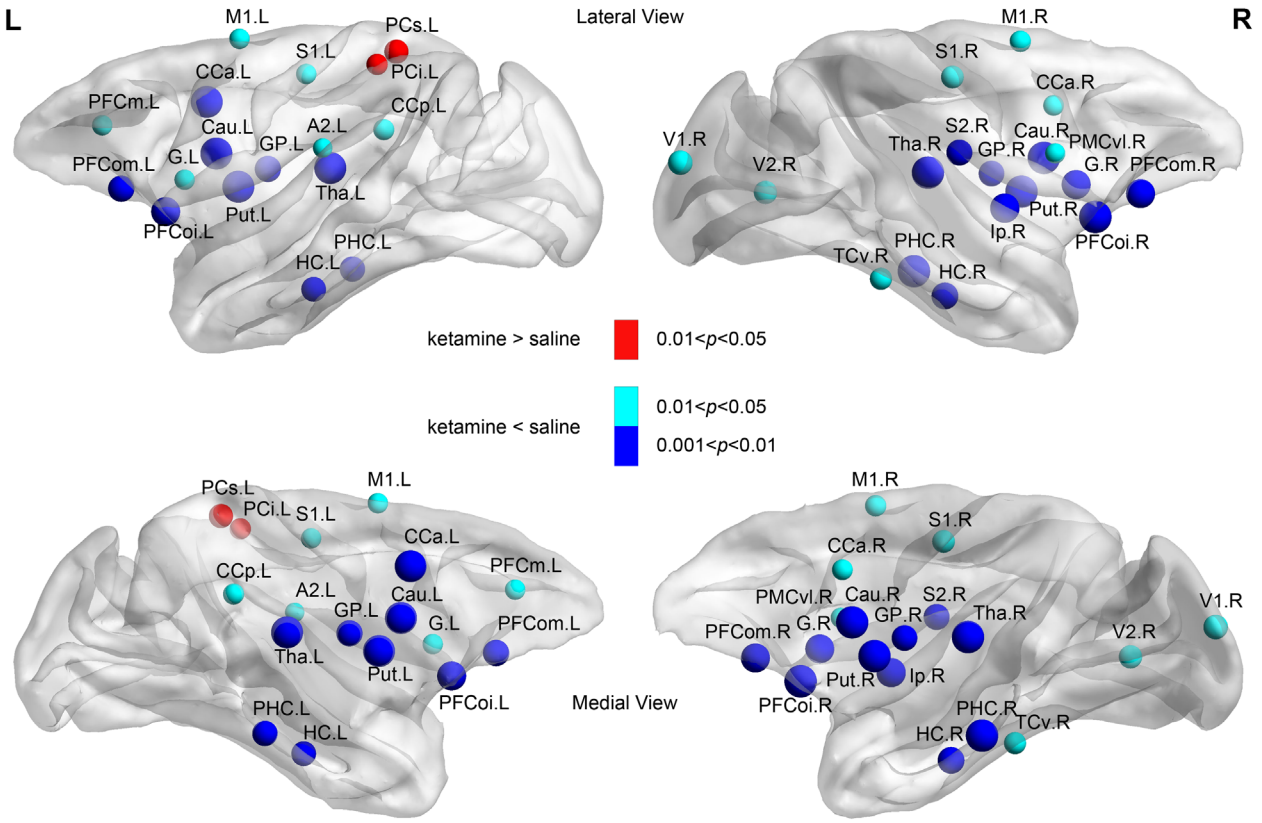

Figure 3. Ketamine-related alterations of nodal strength in functional brain network. Spheres in warm (red) or cold (teal and dark blue) colors indicate brain regions with increased or decreased nodal strength in response to ketamine intake. Size of the spheres represents statistical significance, $-\log_{10}(p)$ (corrected for multiple comparisons). See Table S2 for details. Brain areas were rendered on the transparent surfaces of the F99 template using BrainNet Viewer software. L, left; R, right. See Supplementary Table S1 for abbreviations of brain regions.

Notably, assessment of the left dorsolateral, polar and centrolateral PFC in ketamine versus saline controls also revealed increased connectivity strength; however, they did not withstand correction for multiple comparisons (FDR-corrected p = .07, p = .09, and p = .10, respectively).

Ketamine-related Regulations of Functional Connectivity

NBS analysis was conducted to characterize the specific features within the network. As shown in Figure 4A, downregulated functional connectivity was persistent among the limbic system (subgenual, retrosplenial, anterior, and posterior cingulate cortices, hippocampus, thalamus, and anterior insula), striatum (NAc, caudate), globus pallidum, OFC and ventrolateral PFC, frontal eye field area, premotor cortex, sensory areas and subareas of the temporal and parietal lobes (see Table S3 in Supplement 1 for each decreased connection ranked by significance level; $p < .05$, corrected for multiple comparison). To illustrate higher order topological reconfiguration of the network, we continued to sort each affected node by the total number of altered connections (i.e., degree of affected nodes) and plotted a schematic diagram according to classic anatomical divisions of the brain (Figure 4B and Table S4). This clearly showed that the subgenual cingulate cortex (also known as Cg25) became a principal ketamine-mediated target because the connectivity between Cg25 and the other 14 brain areas (both hemispheres) decreased significantly in response to ketamine intake. Top-ranked brain regions targeted by this NMDA receptor antagonist also included NAc and PCC, each of which had more than nine decreased connections to other structures. Another pronounced feature in Figure 4B is the preponderant down-regulation of the frontocingulate and cingulate-striatal pathways among all altered connections. These results are compatible with the predictive role of the frontocingulate circuit postulated in MDD treatment response (47).

Overall Ketamine-related Regulations of Functional Brain Networks

Taking both node and edge results into account (see Table S5 in Supplement 1 for combination criteria), we found large-scale robust reconfiguration of the whole-brain functional network 18 hours after ketamine administration (Figure 5). The most obviously affected areas, such as the OFC, Cg25, NAc, and PCC, were located predominantly within the cortical-limbic-striatal loops. Overall marked reduction in coherent neural activity was observed primarily in the limbic system (Figure 5, deep blue regions). By contrast, limited cortical areas involving superior and inferior parietal cortices exhibited upregulation of functional connectivity.

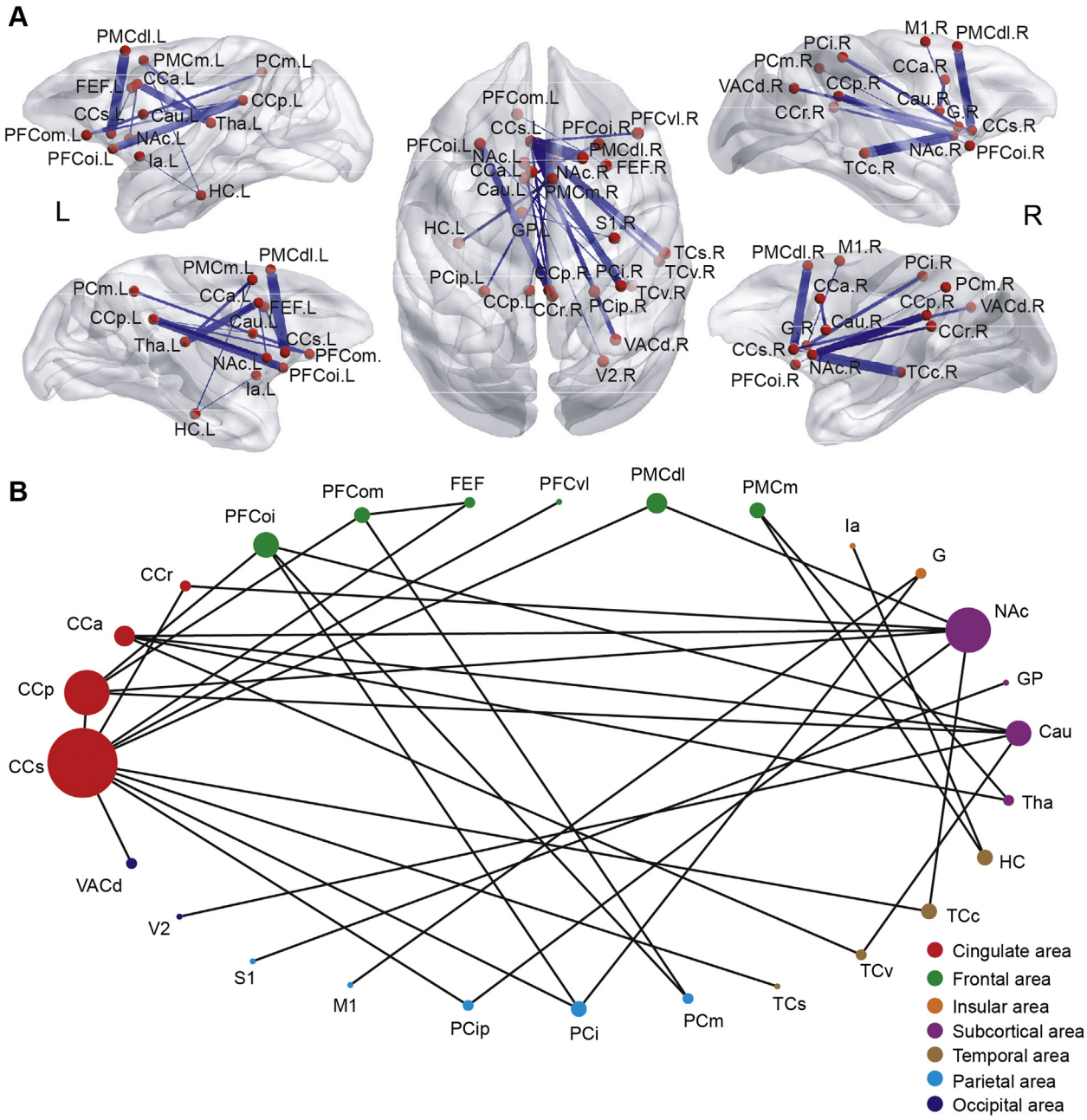

Figure 4. Ketamine-related decrease in functional connectivity. **(A)** Significantly decreased intra- (left and right panels for left and right hemispheres, respectively) and interhemisphere (middle panel) functional connectivity. Thickness of lines representing decreased functional connectivity was scaled with the statistical significance, $-\log_{10}(p)$. **(B)** A hierarchical diagram of the altered connections and connected brain regions in **A** was plotted to present higher order topological reconfiguration evoked by ketamine. Size of spheres indicated the degree of relevant brain areas (i.e., number of decreased connections with other regions). All involved brain regions (including left and right hemispheres) were depicted on a ring and categorized (color-coded) by anatomical locations. See Table S3 for more information. L, left; R, right. See Supplementary Table S1 for abbreviations of brain regions.

DISCUSSION

Global Regulation of Small-World Networks

The brain is organized in an economical small-world architecture that supports both functional integration and segregation (36,41,44), although this delicate balance in brain networks can be vulnerable to disruption by various pathological processes. Previous studies provide consistent evidence of deviant topological organization of functional brain networks in depressed patients, characterized by decreased path length (L_p and λ) and increased global efficiency (E_{glob}) (46,48). Strikingly, in the present study, sustained regulation of the functional network integration induced by ketamine in normal monkeys was exactly opposite to the maladaptive alterations observed in

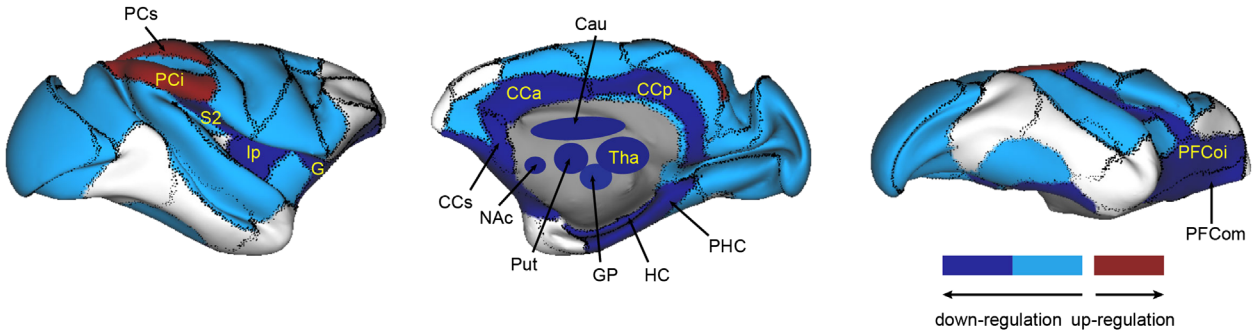

Figure 5. Overall illustration of affected macaque brain regions shown by lateral (left), medial (middle), and ventral (right) views of the right hemisphere. Brain regions were anatomically defined according to the regional map by Bezgin. Levels of downregulation (cold colors) and upregulation (warm colors) were defined on the basis of the node (Figure 3) and edge (Figure 4) results (see Supplement 1 for detailed rules). The most prominent up- and down-regulated brain regions were labelled. Caret software was used to visualize the results on the macaque brain surfaces with inflated F99 template. See supplementary Table S1 for abbreviations of brain regions.

MDD patients (49). This indicates that a single exposure to ketamine may restore the brain's capacity for functional information integration for a prolonged period by reversing the impaired network integration in depression. We also found significant decreases in network metrics representing brain segregation (C_p and E_{loc}), which has not been reported in depressed patients previously. We propose that chronic recovery of MDD is concomitant with normalized balance between functional integration and segregation, which can be achieved by ketamine-mediated network reconfiguration.

At the network level, numerous rsfMRI studies in clinical patients have suggested a crucial role of increased connectivity within the "default-mode network" (DMN) in the pathophysiology of major depression (46,50–52), because DMN is supposed to subserve episodic memory retrieval and self-referential cognition and is behaviorally linked to the ruminative nature of depression in patients. A recent study demonstrated that 10 weeks of treatment with duloxetine normalized the abnormally increased coherence of neural activity within the DMN network in patients with dysthymia (53). Remarkably, the downregulated regions involving the medial PFC, PCC, and rostral and medial temporal lobes, identified by our network approach (rather than a priori seed-based correlation) constituted the main nodes of DMN reported previously in monkeys (19,28). It is interesting to speculate that single-dose ketamine treatment caused specific network-targeted downregulation, which may lead to the normalization of DMN connectivity in depression, thereby contributing to the relief of specific symptom like rumination.

Previous studies showed that ketamine rapidly induced synaptogenesis and reversed structural and functional deficits resulting from long-term stress exposure (7,11). Our results provide the first imaging evidence at the macroscopic scale suggesting that local synaptic alterations triggered by the transient blockade of NMDA receptors were able to translate into a sustained global reconfiguration of neural networks, counteracting the disrupted topological organization in depression.

Regional Regulation of Small-World Networks

Although NMDA receptors are ubiquitous in the entire brain (14) and immediate ketamine action is blockage of NMDA receptors, we demonstrated a highly heterogeneous, persistent ketamine-related activity pattern showing that downregulation was prominently distributed in the OFC, striatum, and primary limbic structures, whereas upregulation was restricted mainly to parts of the parietal cortex. A wealth of evidence has revealed depression-related abnormalities in structural architecture, metabolic activity and functional connectivity within the OFC (1,54), PCC (1,51), ACC (47,55), striatum (1,56), and inferior parietal cortex (5,46). Our results showed that ketamine not only prioritized its targets in the cortical-limbic-striatal loops but also exerted target-specific regulation by reversing local alterations of the networks caused by illness. Notably, changes in both nodal strength and edge connection occurred in the thalamus, which plays a vital role in the pathophysiology of mood disorders (1). Due to limited spatial resolution here, we could not assess the potential effects involving the habenula (included in the thalamus node), a region heavily implicated in the depression circuit (57) and demonstrated in our recent work (58).

The fact that the key ketamine targets identified here, including Cg25, NAc, and PCC, are central to prevailing theories of heuristic depression circuits is of considerable interest (Figure 4B) (1,2,5,59). Functionally interactive networks of corticostriatal and corticolimbic pathways are critical to integrate mood and associate visual, motor, somatic, and cognitive behaviors (1). As key players in the cortico-limbic-striatal loop, Cg25 and NAc are actively involved in autonomic and homeostatic processes (3,60), as well as in emotional and cognitive control (3,59). Furthermore, both have been observed to be metabolically hyperactive in MDD patients (2,50,59). Deep brain stimulation (DBS) in the Cg25 of refractory MDD patients successfully lowered hyperactivity in the Cg25, OFC, and medial PFC, leading to remarkable clinical improvements (60,61). Furthermore, DBS in the ventral striatum (mainly NAc) also significantly decreased activity in the OFC, Cg25, PCC, thalamus, and caudate nucleus (62). Regulation of glutamatergic inputs to the NAc from the Cg25, medial PFC, hippocampus and insula, where resting-state hyperconnectivity was reported in MDD patients (1,52), could undertake a central role in rapidly alleviating anhedonia in depression. The action of ketamine observed here is congruent with current literature supporting the role of Cg25 activity as a promising predictor of antidepressant response.

We further observed that many local brain regions were profoundly affected by ketamine. Specifically, ketamine

selectively downregulated the medial PFC (albeit upregulation in the lateral PFC was not statistically significant after FDR correction) (Figure 3), which tends to enhance voluntary control of emotion generation and regulation but attenuate sensory-related reward processing (2,3,63). The dorsolateral PFC and inferior parietal cortex have been shown to be hypoactivated in depression (5), and DBS treatment in the Cg25 actually increased functional activity in the dorsolateral PFC and inferior parietal cortex (61). Upregulation of these two regions implies improved cognitive control over the vegetative-somatic part (5). Taken together, differential modulation in subdivisions of the PFC exerted by drug treatment is anticipated to achieve equivalent beneficial outcomes acquired by DBS therapy. This points to an important selective pathway through which ketamine may rectify malfunctioning emotion generation, procession and regulation in depression. Nevertheless, the underlying mechanisms of how local synaptic alterations evolve into discriminative regulation within the PFC need future investigation.

Several limitations in interpreting the present results should be considered. The effects of isoflurane, the most commonly used anesthetic in monkeys, could be reflected as changes in the correlation strength between brain areas, localization, or inclusion of distributed nodes within specific networks (19,28). However, recent research has shown that within a carefully controlled narrow range of isoflurane levels, such as ± .26% in our study, statistical coupling between brain areas was consistent and reliable for investigation of functional brain architecture (19,26). Moreover, we argue the potential effect of anesthetic agents was removed by contrasting the saline and ketamine treatments in the same group subjects and the thresholds for network construction were applied uniformly to each subject in both conditions. However, overinterpretation of the present findings from healthy subjects should be kept in mind (49,64–66) until monkey models of mood disorders, such as depression and anxiety, have been developed (30) and used under the same experimental protocol. It was reported previously that schizophrenia-like symptoms can be induced by acute ketamine administration (67), although after a delay period (< 5 hours), the psychotomimetic effects do not last long in monkeys (32). Hence, our findings were not likely contaminated with such an effect as the monkeys were scanned 18 hours after administration. This study did not examine the neural origin of the sustained effects imposed by the action of ketamine, which needs to be addressed with the help of neurophysiological recordings. Further, the link between the neurobiological alterations and the graph network-model differences is missing, which definitely merits future work to clarify and validate.

Conclusions

In summary, our whole-brain analyses revealed large-scale network reconfiguration of the distributed cortico-limbic-striatal circuits, an effect visible at least 18 hours after application. Strikingly, the ketamine-induced activity patterns precisely opposed the maladaptive activity in the depressed brain, suggesting that ketamine may mediate its antidepressant effects in multiple behavior domains. Our findings pave a new avenue to understand the mechanisms underlying the efficacy of antidepressant action and to aid the development of improved therapeutics that guide plastic synaptic connections in these key areas analogically targeted by ketamine.

ACKNOWLEDGEMENTS AND DISCLOSURES

This work was supported by the Hundred Talent Program of the Chinese Academy of Sciences (Technology) (ZW), the Chinese 973 Program (2011CBA00400), the Strategic Priority Research Program (B) of the Chinese Academy of Sciences (XDB02030004), and the Outstanding Youth Grant of the National Natural Science Foundation of China (HH).

The authors thank Drs. Mu-ming Poo, Richard Tsien, Anna Roe, and R. Matthew Hutchison for their insightful comments on the manuscript and related topics; and Drs. Lawrence Wald, Ravi Menon, John Gore, Franz Schmitt, Renate Jerecic, Thomas Benner, Kecheng Liu, Ignacio Vallines, and Hui Liu for their generous help and contribution to the construction of our custom-tuned gradient-insert (AC88) 3T MRI facility for nonhuman primate subjects.

A portion of this work was reported in abstract form at the Annual Meeting of the Society for Neuroscience, November 17, 2014, Washington, DC.

All authors declare no biomedical financial interests or potential conflicts of interest.

ARTICLE INFORMATION

From the Key Laboratory of Primate Neurobiology (QL, LY, ZW, ZS, WY, QJ, BH, JP, HH, ZW), Institute of Neuroscience, Shanghai Institute for Biological Sciences, Chinese Academy of Sciences, Shanghai, China; and Department of Anesthesiology (GL), Zhongshan Hospital, Fudan University, Shanghai, China.

QL and LY contributed equally to this work.

HH and ZW contributed equally to this work.

Address correspondence to Zheng Wang, 320 Yueyang Road, Shanghai 200031, China; E-mail: zheng.wang@ion.ac.cn.

Received Sep 25, 2014, revised Jan 13, 2015; accepted Feb 15, 2015.

Supplementary material cited in this article is available online at http://dx.doi.org/10.1016/j.biopsych.2015.02.028.

REFERENCES

1. Price JL, Drevets WC (2010): Neurocircuitry of mood disorders. Neuropsychopharmacology 35:192–216.
2. Sesack SR, Grace AA (2010): Cortico-basal ganglia reward network: microcircuitry. Neuropsychopharmacology 35:27–47.
3. Krishnan V, Nestler EJ (2010): Linking molecules to mood: new insight into the biology of depression. Am J Psychiatry 167:1305–1320.
4. Castren E (2013): Neuronal network plasticity and recovery from depression. JAMA Psychiatry 70:983–989.
5. Mayberg HS, Liotti M, Brannan SK, McGinnis S, Mahurin RK, Jerabek PA, *et al*. (1999): Reciprocal limbic-cortical function and negative mood: converging PET findings in depression and normal sadness. Am J Psychiatry 156:675–682.
6. Nestler EJ, Carlezon WA Jr (2006): The mesolimbic dopamine reward circuit in depression. Biol Psychiatry 59:1151–1159.
7. Duman RS, Aghajanian GK (2012): Synaptic dysfunction in depression: potential therapeutic targets. Science 338:68–72.
8. Berman RM, Cappiello A, Anand A, Oren DA, Heninger GR, Charney DS, *et al*. (2000): Antidepressant effects of ketamine in depressed patients. Biol Psychiatry 47:351–354.
9. Zarate CA Jr, Singh JB, Carlson PJ, Brutsche NE, Ameli R, Luckenbaugh DA, *et al*. (2006): A randomized trial of an *N*-methyl-D-aspartate antagonist in treatment-resistant major depression. Arch Gen Psychiatry 63:856–864.
10. Price RB, Nock MK, Charney DS, Mathew SJ (2009): Effects of intravenous ketamine on explicit and implicit measures of suicidality in treatment-resistant depression. Biol Psychiatry 66:522–526.

11. Autry AE, Adachi M, Nosyreva E, Na ES, Los MF, Cheng PF, *et al*. (2011): NMDA receptor blockade at rest triggers rapid behavioural antidepressant responses. Nature 475:91–95.
12. Li N, Lee B, Liu RJ, Banasr M, Dwyer JM, Iwata M, *et al*. (2010): mTOR-dependent synapse formation underlies the rapid antidepressant effects of NMDA antagonists. Science 329:959–964.
13. Murrough JW, Perez AM, Pillemer S, Stern J, Parides MK, aan het Rot M, *et al*. (2013): Rapid and longer-term antidepressant effects of repeated ketamine infusions in treatment-resistant major depression. Biol Psychiatry 74:250–256.
14. Sanacora G, Zarate CA, Krystal JH, Manji HK (2008): Targeting the glutamatergic system to develop novel, improved therapeutics for mood disorders. Nat Rev Drug Discov 7:426–437.
15. Zunszain PA, Horowitz MA, Cattaneo A, Lupi MM, Pariante CM (2013): Ketamine: synaptogenesis, immunomodulation and glycogen synthase kinase-3 as underlying mechanisms of its antidepressant properties. Mol Psychiatry 18:1236–1241.
16. Krystal JH, Sanacora G, Duman RS (2013): Rapid-acting glutamatergic antidepressants: the path to ketamine and beyond. Biol Psychiatry 73:1133–1141.
17. Aan Het Rot M, Zarate CA Jr, Charney DS, Mathew SJ (2012): Ketamine for depression: where do we go from here? Biol Psychiatry 72:537–547.
18. Sinner B, Graf BM (2008): Ketamine. Handb Exp Pharmacol 182: 313–333.
19. Vincent JL, Patel GH, Fox MD, Snyder AZ, Baker JT, Van Essen DC, *et al*. (2007): Intrinsic functional architecture in the anaesthetized monkey brain. Nature 447:83–86.
20. Margulies DS, Vincent JL, Kelly C, Lohmann G, Uddin LQ, Biswal BB, *et al*. (2009): Precuneus shares intrinsic functional architecture in humans and monkeys. Proc Natl Acad Sci U S A 106:20069–20074.
21. Matsui T, Tamura K, Koyano KW, Takeuchi D, Adachi Y, Osada T, *et al*. (2011): Direct comparison of spontaneous functional connectivity and effective connectivity measured by intracortical microstimulation: an fMRI study in macaque monkeys. Cereb Cortex 21: 2348–2356.
22. Logothetis NK, Eschenko O, Murayama Y, Augath M, Steudel T, Evrard HC, *et al*. (2012): Hippocampal-cortical interaction during periods of subcortical silence. Nature 491:547–553.
23. Hutchison RM, Womelsdorf T, Gati JS, Everling S, Menon RS (2013): Resting-state networks show dynamic functional connectivity in awake humans and anesthetized macaques. Hum Brain Mapp 34: 2154–2177.
24. Wang Z, Chen LM, Negyessy L, Friedman RM, Mishra A, Gore JC, *et al*. (2013): The relationship of anatomical and functional connectivity to resting-state connectivity in primate somatosensory cortex. Neuron 78:1116–1126.
25. Mars RB, Jbabdi S, Sallet J, O'Reilly JX, Croxson PL, Olivier E, *et al*. (2011): Diffusion-weighted imaging tractography-based parcellation of the human parietal cortex and comparison with human and macaque resting-state functional connectivity. J Neurosci 31: 4087–4100.
26. Hutchison RM, Hutchison M, Manning KY, Menon RS, Everling S (2014): Isoflurane induces dose-dependent alterations in the cortical connectivity profiles and dynamic properties of the brain's functional architecture. Hum Brain Mapp 35:5754–5775.
27. Sallet J, Mars RB, Noonan MP, Neubert FX, Jbabdi S, O'Reilly JX, *et al*. (2013): The organization of dorsal frontal cortex in humans and macaques. J Neurosci 33:12255–12274.
28. Hutchison RM, Everling S (2012): Monkey in the middle: why non-human primates are needed to bridge the gap in resting-state investigations. Front Neuroanat 6:29.
29. Groman SM, Jentsch JD (2013): Identifying the molecular basis of inhibitory control deficits in addictions: neuroimaging in non-human primates. Curr Opin Neurobiol 23:625–631.
30. Berton O, Hahn CG, Thase ME (2012): Are we getting closer to valid translational models for major depression? Science 338:75–79.
31. Capitanio JP, Emborg ME (2008): Contributions of non-human primates to neuroscience research. Lancet 371:1126–1135.
32. Gil-da-Costa R, Stoner GR, Fung R, Albright TD (2013): Nonhuman primate model of schizophrenia using a noninvasive EEG method. Proc Natl Acad Sci U S A 110:15425–15430.
33. Driesen NR, McCarthy G, Bhagwagar Z, Bloch MH, Calhoun VD, D'Souza DC, *et al*. (2013): The impact of NMDA receptor blockade on human working memory-related prefrontal function and connectivity. Neuropsychopharmacology 38:2613–2622.
34. Scheidegger M, Walter M, Lehmann M, Metzger C, Grimm S, Boeker H, *et al*. (2012): Ketamine decreases resting state functional network connectivity in healthy subjects: implications for antidepressant drug action. PLoS One 7:e44799.
35. Gass N, Schwarz AJ, Sartorius A, Schenker E, Risterucci C, Spedding M, *et al*. (2014): Sub-anesthetic ketamine modulates intrinsic BOLD connectivity within the hippocampal-prefrontal circuit in the rat. Neuropsychopharmacology 39:895–906.
36. Bullmore E, Sporns O (2009): Complex brain networks: graph theoretical analysis of structural and functional systems. Nat Rev Neurosci 10:186–198.
37. Zalesky A, Fornito A, Bullmore ET (2010): Network-based statistic: identifying differences in brain networks. Neuroimage 53:1197–1207.
38. Yamamoto S, Ohba H, Nishiyama S, Harada N, Kakiuchi T, Tsukada H, *et al*. (2013): Subanesthetic doses of ketamine transiently decrease serotonin transporter activity: a PET study in conscious monkeys. Neuropsychopharmacology 38:2666–2674.
39. Van Essen DC, Drury HA, Dickson J, Harwell J, Hanlon D, Anderson CH (2001): An integrated software suite for surface-based analyses of cerebral cortex. J Am Med Inform Assoc 8:443–459.
40. Rohlfing T, Kroenke CD, Sullivan EV, Dubach MF, Bowden DM, Grant KA, *et al*. (2012): The INIA19 template and NeuroMaps atlas for primate brain image parcellation and spatial normalization. Front Neuroinform 6:27.
41. Achard S, Bullmore E (2007): Efficiency and cost of economical brain functional networks. PLoS Comput Biol 3:174–183.
42. Bassett DS, Bullmore E, Verchinski BA, Mattay VS, Weinberger DR, Meyer-Lindenberg A (2008): Hierarchical organization of human cortical networks in health and schizophrenia. J Neurosci 28: 9239–9248.
43. Watts DJ, Strogatz SH (1998): Collective dynamics of 'small-world' networks. Nature 393:440–442.
44. Rubinov M, Sporns O (2010): Complex network measures of brain connectivity: uses and interpretations. Neuroimage 52:1059–1069.
45. Maslov S, Sneppen K (2002): Specificity and stability in topology of protein networks. Science 296:910–913.
46. Zhang J, Wang J, Wu Q, Kuang W, Huang X, He Y, *et al*. (2011): Disrupted brain connectivity networks in drug-naive, first-episode major depressive disorder. Biol Psychiatry 70:334–342.
47. Pizzagalli DA (2011): Frontocingulate dysfunction in depression: toward biomarkers of treatment response. Neuropsychopharmacology 36:183–206.
48. Leistedt SJ, Coumans N, Dumont M, Lanquart JP, Stam CJ, Linkowski P (2009): Altered sleep brain functional connectivity in acutely depressed patients. Hum Brain Mapp 30:2207–2219.
49. Ma Y. (2014): Neuropsychological mechanism underlying antidepressant effect: a systematic meta-analysis. Mol Psychiatry 20:311–319.
50. Greicius MD, Flores BH, Menon V, Glover GH, Solvason HB, Kenna H, *et al*. (2007): Resting-state functional connectivity in major depression: abnormally increased contributions from subgenual cingulate cortex and thalamus. Biol Psychiatry 62:429–437.
51. Sheline YI, Price JL, Yan Z, Mintun MA (2010): Resting-state functional MRI in depression unmasks increased connectivity between networks via the dorsal nexus. Proc Natl Acad Sci U S A 107:11020–11025.
52. Hasler G, Northoff G (2011): Discovering imaging endophenotypes for major depression. Mol Psychiatry 16:604–619.
53. Posner J, Hellerstein DJ, Gat I, Mechling A, Klahr K, Wang Z, *et al*. (2013): Antidepressants normalize the default mode network in patients with dysthymia. JAMA Psychiatry 70:373–382.
54. Frodl T, Bokde AL, Scheuerecker J, Lisiecka D, Schoepf V, Hampel H, *et al*. (2010): Functional connectivity bias of the orbitofrontal cortex in drug-free patients with major depression. Biol Psychiatry 67:161–167.

55. Hasler G, Drevets WC, Manji HK, Charney DS (2004): Discovering endophenotypes for major depression. Neuropsychopharmacology 29:1765–1781.
56. Meng C, Brandl F, Tahmasian M, Shao JM, Manoliu A, Scherr M, *et al*. (2014): Aberrant topology of striatum's connectivity is associated with the number of episodes in depression. Brain 137:598–609.
57. Li B, Piriz J, Mirrione M, Chung C, Proulx CD, Schulz D, *et al*. (2011): Synaptic potentiation onto habenula neurons in the learned helplessness model of depression. Nature 470:535–539.
58. Li K, Zhou T, Liao L, Yang Z, Wong C, Henn F, *et al*. (2013): betaCaMKII in lateral habenula mediates core symptoms of depression. Science 341:1016–1020.
59. Hamani C, Mayberg H, Stone S, Laxton A, Haber S, Lozano AM (2011): The subcallosal cingulate gyrus in the context of major depression. Biol Psychiatry 69:301–308.
60. Mayberg HS (2009): Targeted electrode-based modulation of neural circuits for depression. J Clin Invest 119:717–725.
61. Mayberg HS, Lozano AM, Voon V, McNeely HE, Seminowicz D, Hamani C, *et al*. (2005): Deep brain stimulation for treatment-resistant depression. Neuron 45:651–660.
62. Bewernick BH, Hurlemann R, Matusch A, Kayser S, Grubert C, Hadrysiewicz B, *et al*. (2010): Nucleus accumbens deep brain stimulation decreases ratings of depression and anxiety in treatment-resistant depression. Biol Psychiatry 67:110–116.
63. Koenigs M, Grafman J (2009): The functional neuroanatomy of depression: distinct roles for ventromedial and dorsolateral prefrontal cortex. Behav Brain Res 201:239–243.
64. Schaefer A, Burmann I, Regenthal R, Arelin K, Barth C, Pampel A, *et al*. (2014): Serotonergic modulation of intrinsic functional connectivity. Curr Biol 24:2314–2318.
65. McCabe C, Mishor Z, Filippini N, Cowen PJ, Taylor MJ, Harmer CJ (2011): SSRI administration reduces resting state functional connectivity in dorso-medial prefrontal cortex. Mol Psychiatry 16:592–594.
66. McCabe C, Mishor Z (2011): Antidepressant medications reduce subcortical-cortical resting-state functional connectivity in healthy volunteers. Neuroimage 57:1317–1323.
67. Krystal JH, Karper LP, Seibyl JP, Freeman GK, Delaney R, Bremner JD, *et al*. (1994): Subanesthetic effects of the noncompetitive NMDA antagonist, ketamine, in humans. Psychotomimetic, perceptual, cognitive, and neuroendocrine responses. Arch Gen Psychiatry 51:199–214.